ASTRONOMY & ASTROPHYSICS
SUPPLEMENT SERIES

Astron. Astrophys. Suppl. Ser. **144**, 169–180 (2000)

Microwave tomography of solar magnetic fields

A. Grebinskij[1], V. Bogod[1], G. Gelfreikh[2], S. Urpo[3], S. Pohjolainen[3], and K. Shibasaki[4]

[1] Special Astrophysical Observatory, S. Petersburg, Russia
[2] Pulkovo Astronomical Observatory, S. Petersburg, Russia
[3] Metsähovi Radio Observatory, Kylmälä, Finland
[4] Nobeyama Radio Observatory, Japan

Received October 28, 1998; accepted February 25, 2000

Abstract. We present a new technique for the measurement of magnetic fields in the solar chromosphere - corona through observations of its free-free microwave emission in intensity and polarization. We derive the decoupled radiation transfer equations for Stoke's parameters of I and V for circular polarized emission in plane-layer inhomogeneous atmospheres and present a model solutions of inversion problem. We discuss the discrimination between contributions from the corona and the chromosphere to the observed brightness spectra from the quiet Sun and plage regions and propose a practical method of magnetic field estimates, which was used both with single frequency (the Nobeyama Radioheliograph at 17 GHz) and multi frequency (RATAN at $1-16$ GHz) observations and discuss the preliminary results. The proposed techniques may be useful as *microwave magnetography* at the corona base and for checks and improvements in the current problem of extrapolating magnetic fields from photosphere to corona.

Key words: polarization — radiative transfer — methods: data analysis Sun: magnetic fields — Sun: radio radiation

1. Introduction

The structure of coronal magnetic fields plays a crucial role in problems of heating and flare energy release, but our knowledge of it is rather limited as compared to photospheric level. The magnetic field in the corona cannot be measured with confidence from Zeeman splitting of coronal lines. Three main techniques are widely discussed in this context (Lee et al. 1998): optical observations of vector magnetic fields in the photosphere and their extrapolation into the corona (McClymont et al. 1997); EUV/X-ray observations which can reveal the projected paths of magnetic field lines via the density contrast between neighboring bundles of field lines (Yan & Sakurai 1997); and spectral-polarization radio observations in the frequency domain of gyroresonance emission mechanism, which are sensitive to both the strength and the direction of the coronal magnetic field (Lang et al. 1993; Abramov–Maximov et al. 1996; Vourlidas et al. 1997; see White & Kundu 1997 for review). These different techniques are complementary, each have its own advantages and disadvantages and should therefore be combined in order to make further progress.

The above techniques are effective when we deal with magnetic fields either at photospheric or the coronal levels, but the crucial intermediate region of the upper chromosphere is not accessible to those studies. Here we try to fill this gap by a detailed analysis of polarization-intensity spectra of free-free (i.e. bremsstrahlung) microwave emission from active regions (Bogod & Gelfreikh 1980). Such techniques, combined with 2D microwave imaging, provide direct microwave magnetograms at the interface between chromosphere and corona (Grebinskij et al. 1998) and may be important for an independent check of chromospheric and coronal fields interpolated from photospheric fields.

The magnetoionic theory (Ratcliffe 1959) predicts two modes of propagating electromagnetic radiation, ordinary and extraordinary, with different opacities. The intensity of polarized emission is proportional to the longitudinal component of the magnetic field, which may be retrieved from spectral-polarization observations by inversion techniques (Gelfreikh 1972). There are several important deficiencies which limit the practical usage of the methods during the past years. The thermal microwave emission from solar active regions is generated by two basic mechanisms, i.e. gyroresonance line (at the second and third harmonic of the electron gyrofrequency $\nu_B = 2.8\ 10^6\ B$ Hz), and free-free continuum emission. Polarization effects for free-free emission at high frequencies are very weak and the circular polarization degree $\rho \equiv V/I$ is

Send offprint requests to: S. Urpo

ranging between 0.1 and 10%, both for weak (prominences, plage areas, coronal holes) and strong (sunspot) fields. At longer wavelengths the polarization increases as $\rho \sim \lambda$ ($V \sim \lambda^3$, $I \sim \lambda^2$) for optically thin emission (Grebinskij 1985). At the frequencies lower then ($\nu \leq 3\nu_B$) the gyroresonance emission becomes dominant above sunspot regions. Thus, the possibilities of measurements (with free-free emission) of magnetic fields at longer cm waves are limited above active regions. The relative contributions of both emission mechanisms were widely discussed in the seventies with the first RATAN, Westerbork and VLA observations (see Alissandrakis et al. 1980 for review). The gyroresonance emission dominates above sunspots at cm waves, where the strong sunspot fields are strongly localized so that the corona is mainly radiating free-free emission above plage regions and between spots (see Gary & Hurford 1994).

Thus, the main domain of free-free emission lies at short cm wavelengths. Observations at $\lambda = 1.76$ cm (Nobeyama Radioheliograph) meet this condition for all active regions with magnetic fields below $B = 2000$ G, which correspond to the third gyroresonance harmonic. In that frequency range the main observational problem concerns the instrumental limitations of measurements of the weak polarization effects. The most existing instruments (OVRO, VLA) acquire and process data in a left-right hand polarization modes and have an insufficient accuracy of polarization measurements above 10%. One-dimensional imaging with RATAN provides a high dynamic range of about 1000:1, but its fan-beam pattern diminishes the observed contrast. Single dish observations (RT-22 of CrAO) have an insufficient angular resolution (minutes of arc). For these instruments only a few reliable results of free-free polarization measurements have been reported: around $\lambda \approx 1$ cm with the RT-22 (CrAO) radio telescope (Apushkinskiy & Topchilo 1976) for polar prominences; at $\lambda = 6$ cm with the WSRT interferometer (Kundu et al. 1977) for plages; at $2.3 - 4.0$ cm with RATAN (Bogod & Gelfreikh 1980) for plage regions; at decimetric wavelength with RATAN (Borovik et al. 1999) for a coronal hole.

This situation has changed with the construction of the Nobeyama Radioheliograph. Its high operation frequency of 17 GHz gives opportunities for studying rather strong fields $B \leq 2000$ G, and its high sensitivity of polarized imaging (with $\rho_{\rm rms} \leq 1\%$) opens possibilities for measuring weak fields also. The design principles of the Nobeyama Radioheliograph (Shibasaki et al. 1991) make it especially appropriate for these goals: (a) its data processing (Hanaoka et al. 1994) is based on the transformation of recorded data (in left-right polarizations) to the Stoke's parameters I, V in the primary processing stage (rough imaging before CLEAN), that gives a high dynamical range (26 dB) both for I and V images, and (b) its high acquisition rate (0.1 s) providing many possibilities for improvement of the images (dynamic range through averaging, resolution enhancements up to 10 arcsec etc.).

The main goal of this paper is to develop the practical methods of solar magnetic field measurements, which are based on an analysis of free-free emission recorded with Nobeyama radio maps (*microwave magnetography*) and RATAN - Metsahovi radiospectroscopy. The method uses an improved treatment of radiation transfer equations and realistic model atmospheres, based on mm waves Metsahovi observations (Urpo et al. 1987). This includes a number of problems, discussed below: the derivation of the decoupled radiation transfer equations for the Stoke's parameters I and V (see Appendix A); the problem of inversion of those equations for the extraction of magnetic fields (Sect. 2); a development of simplified model atmospheres to distinguish contributions of the chromosphere and the corona in the observed spectra (Sect. 3); the development of practically estimates of magnetic fields (Sect. 4).

We illustrate and discuss these techniques with results of published and new (Nobeyama) observations (Sects. 5 and 6). Some further results, related to the study of strong sunspot fields with Nobeyama imaging, will be discussed separately (see Grebinskij et al. 1998).

2. Radiation transfer in inhomogeneous atmospheres

In order to retrieve magnetic field from intensity and polarization spectra emitted by an inhomogeneous solar atmosphere we use the radiation transfer equations for the Stoke's parameters of total intensity $I = (T_{\rm r}^+ + T_{\rm r}^-)/2$ and $V = (T_{\rm r}^+ - T_{\rm r}^-)/2$ for circular polarization. These equations for the bremsstrahlung emission mechanism in an inhomogeneous plane layered atmosphere (see Appendix A) are:

$$I(\lambda) = \lambda^2 \int\limits_0^\infty T_{\rm e}(t) {\rm e}^{-\lambda^2 t} {\rm d}t, \tag{1}$$

$$V(\lambda) = \lambda^2 \int\limits_0^\infty \beta(t) \triangle T(t) {\rm e}^{-\lambda^2 t} {\rm d}t,$$

$$\triangle T(t) = \int\limits_0^\infty \frac{{\rm d}T_{\rm e}(t+t')}{{\rm d}t} {\rm e}^{-\lambda^2 t'} {\rm d}t', \tag{2}$$

where $\beta = 2\nu_B \cos\alpha/\nu \ll 1$, $\nu_B = 2.8\ 10^6 B$ is the electron gyrofrequency, $\nu = c/\lambda$, α is the angle between the magnetic field vector $\boldsymbol{B}$ and the line of sight and $T_{\rm e}$ is the electron temperature. The integration is carried out with respect to the argument t, the frequency-independent radio depth measure as a function of the current geometrical depth l from the top, based on the isotropical optical depth $\tau(l)$

$$t \equiv \frac{\tau(l)}{\lambda^2} = \frac{1}{\lambda^2} \int\limits_0^l \mu^{\rm o}(l'){\rm d}l' \propto \int\limits_0^l \frac{N_{\rm e}^2}{T_{\rm e}^{3/2}} {\rm d}l', \tag{3}$$

where $\mu^{o} \simeq 0.2 \cdot \nu^{-2} N_e^2 T_e^{-3/2}$ is the bremsstrahlung opacity in an isotropic plasma with electron density N_e.

The solution of the inverse problem given by Eqs. (1), (2) gives the magnetic field $B \equiv (5350/\lambda)\beta(t)$ and the electron temperature $T_e(t)$ in the solar atmosphere as functions of t. We call such solutions "tomographic" models (see Bogod & Grebinskij 1997) because they represent the only direct information, which may be extracted from brightness spectra without additional assumptions. The "physical" models, i.e. spatial distributions of the electron number density $N_e(h)$, electron temperature $T_e(h)$ and field $B(h)$, may be retrieved from the tomographic models by solving the inversion problem Eq. (3), which requires the assumptions on the relation between $T_e(h)$ and $N_e(h)$. This approach is quite different from the standard model method which starts with the information obtained from optical observations and then does forward calculations to fit microwave observations in the following steps: $T_e(h)$, $N_e(h) \Rightarrow t(T_e) \Rightarrow T_e(t) \Rightarrow T_b(\nu)$ (see Avrett 1997 for review).

It was shown by Bogod & Grebinskij (1997), that Eq. (1) may be effectively inverted to find $T_e(t)$ by the differential deconvolution method (DDM). However, that technique is not applicable to Eq. (2), which cannot be reduced to a Laplace transform. Thus, to retrieve magnetic fields from spectral observations, we should use some estimates, well known from previous studies by Bogod & Gelfreikh (1980) in the form of (see Appendix A):

$$[\beta(\lambda)] = \frac{V_{obs}(\lambda)}{\lambda^2 \mathrm{d}I_{obs}/\mathrm{d}(\lambda^2)}, \quad [B(\lambda)]_G \equiv \frac{5350}{\lambda_{cm}}[\beta(\lambda)]. \qquad (4)$$

Here and below we use the square brackets to denote physical qualities, which are obtained by inversion from radio brightness spectra and to distinguish its presumed physical values (denoted without square brackets) in the atmosphere. This expression gives an exact solution of Eqs. (1), (2) for any inhomogeneous atmosphere with uniform magnetic field (see Appendix A).

In order to obtain such estimates from observations of solar atmosphere emission in the case of inhomogeneous magnetic fields, one should answer on two questions: (i) Which layer of the atmosphere (corona or chromosphere) gives the main contribution to the polarization at a given wavelength λ? (ii) What is the relation between the estimated magnetic field $[B(\lambda)]$ (Eq. 4) and its real value in the case of an inhomogeneous field $B(h)$?

In order to answer these questions, we use a priori information about the distribution of temperature in the solar atmosphere, which may be extracted from observed brightness spectra by Eq. (1) and modelling.

3. Origin of polarization in the solar atmosphere

Brightness contrasts above the magnetic network from recent VLA - Yohkoh (SXT) observations of quiet Sun regions with arc sec resolution (at λ = 1.3, 2.0, and 3.6 cm) were obtained by Benz et al. (1997). Model simulations with current optical reference atmospheres (Fontenla et al. 1993) were inconclusive. In order to solve the problems of model simulations we use here the results of a multi frequency study (Bogod & Grebinskij 1997) in a wide range of mm − cm band microwave brightness observations with moderate (arcmin) spatial resolution.

3.1. Model simulations of the quiet Sun and plage emission

The solar atmosphere at microwave frequencies can be considered (see Grebinskij 1987; Zirin et al. 1991) as a two-component medium with an optically thin corona and an optically thick chromosphere with small temperature gradients:

$$T_b(\lambda) = T_{e,cor}\tau_{cor}(\lambda) + T_{b,chr}(\lambda). \qquad (5)$$

Zirin et al. (1991) found the best fit to the quiet Sun brightness spectra with $T_b = 140077 \cdot \nu^{-2.1} + 10880$ K in the frequency range $1.4 - 18$ GHz, which corresponds to an optically thick and isothermal chromosphere with $T_{e,chr}$ = 10880 K. Bogod & Grebinskij (1997) used a wider frequency range (1−90 GHz) and reported a slight power-law chromosphere electron temperature gradient $T_{e,chr}(t) \sim t^{-q}$ from the inversion of the chromosphere emission spectrum at the short microwave lengths ($\lambda < 3$ cm) for the quiet Sun and plage regions. We simulate these spectra by using a two component model (slightly anisothermic chromosphere and optically thin corona) of the solar atmosphere with several free parameters. Here, we would totally neglect all possible contributions to observed microwave emission from a solar plasma at transition temperature range. The matter of plasma is confined into unresolved small scale loops (see Grebinskij 1987 and Appendix B). For coronal layers the coronal brightness temperature follows:

$$\begin{aligned} T_{b,cor}(\lambda) &= \lambda^2 < tT_e >_{cor}, \\ &< tT_e >_{cor} \equiv \int_0^{t_{cor}} T_e(t)\mathrm{d}t, \end{aligned} \qquad (6)$$

where $< tT_e >_{cor}$ is related to the column emission measure $EM(T_c) = \int N_e^2 dl$ according to $< tT_e >_{cor} \simeq 2\ 10^{-22} EM_{cor} T_c^{-0.5}$ and can be directly determined by the inversion of observed brightness spectra (see Bogod & Grebinskij 1997).

For the chromosphere, we use a power-law electron temperature distribution, as

$$T_{e,chr}(t) = \begin{cases} T_o, & t \le t_o \\ T_o(\frac{t}{t_o})^{-q}, & t \ge t_o \end{cases}. \qquad (7)$$

Table 1. Radio brightness excesses of plage areas, observed and modelled

λ [cm]	Observed T_{QS} (10^3 K)	Observed ΔT_{PL} (10^3 K)	Reference	Modelled T_{QS} (10^3 K)	Modelled ΔT_{PL} (10^3 K)	n_{PL}
0.37	7.25	1.0	(Urpo et al. 1987)	7.24	1.1	0.22
0.82	7.8	2.1	(same)	8.46	1.7	0.29
1.35	9.0	6.0	(same)	9.46	2.8	0.41
1.76	10.0	4 – 6	(Nobeyama, this paper)	10.1	4.0	0.52
2.0	10.2	3.5	(Bogod & Gelfreikh 1980)	10.5	4.7	0.59
2.3	10.9	4.8	(same)	10.9	5.8	0.67
2.7	11.6	6.4	(same)	11.6	7.5	0.78
3.2	12.6	9.6	(same)	12.3	10	0.93
4.0	15.0	12.5	(same)	13.6	15	1.09
6.0	20.0	30 – 40	(Kundu et al. 1977)	17.4	31	1.41
13.0	42.5	89	(Akhmedov et al. 1987)	37.2	130	1.81
21.0	90	288	(same)	70.9	310	1.91

The modelled brightness spectrum of the chromosphere is obtained from Eqs. (1) and (7)

$$T_{\rm b,chr}(\lambda) = T_{\rm o}(1-{\rm e}^{-\tau_{\rm o}}) + T_{\rm o}\tau_{\rm o}^{q}\Gamma(1-q,\tau_{\rm o}), \quad \tau_{\rm o} \equiv \lambda^2 t_{\rm o}, \tag{8}$$

where Γ is the partial Euler Gamma function. Our model chromosphere is justified by the following reasons. For a power-law kinetic temperature distribution (Eq. 7) in the chromosphere the emission brightness temperature $T_{\rm b,chr}(\lambda)$ at fixed λ_* corresponds to the electron temperature at the level with $\tau(\lambda_*) \simeq 1$, or $t_* \simeq \lambda_*^{-2}$. From Eq. (7) we find $T_{\rm b,chr}(\lambda_*) \simeq T_{\rm e,chr}(t_*) = T_{\rm o}(t_{\rm o}\lambda_*^2)^q$ with the power-law brightness spectrum with spectral index $n = 2q$. Thus, in order to match the observations, one should use: (i) the temperature index q, which is mostly defined by the shape of the observed brightness spectrum at the short microwave lengths; (ii) the chromospheric temperature parameter $T_{\rm o}$, which is the expected value of the electron temperature at the top of the chromosphere ($T_{\rm e} \simeq 10 - 20\ 10^3$ K); (iii)the final adjustment of the optical depth scale $t_{\rm o}$ of the electron temperature $T_{\rm e}(t)$ with the chromosphere depth t.

The model has 4 free parameters ($T_{\rm o}, t_{\rm o}, q$ and $< tT_{\rm e} >_{\rm cor}$). The same model is used both for the quiet Sun and plage emission, but with different parameters. These are found by modelling the observed brightness spectra.

As observational spectra for model matching, we use here a combination of OVRO (Zirin et al. 1991) and compiled (Bogod & Grebinskij 1997) mm-band observations for different quiet Sun regions (as reference) in the frequency range of 87 – 1.4 GHz. For plage area(s) we use observations from Metsähovi at 87 – 22 GHz (Urpo et al. 1987), Nobeyama maps at 17 GHz, RATAN at 1.4–16 GHz (Bogod & Gelfreikh 1980; Akhmedov et al. 1982), and Westerbork at 5 GHz (Kundu et al. 1977). With plage data we use the reported results of reduction of observed brightness excesses for moderate beam resolution.

The results of the brightness spectra simulations are well fitted by simple model with the following parameters:

$$\begin{aligned} \text{Quiet Sun}: \quad & T_{\rm o} = 15000\ {\rm K}, \quad t_{\rm o} = 10^{-2.5}, \\ & q = 0.095, \quad < tT >_{\rm cor} = 95. \end{aligned} \tag{9}$$

$$\begin{aligned} \text{Plage}: \quad & T_{\rm o} = 15000\ {\rm K}, \quad t_{\rm o} = 10^{-1.9}, \\ & q = 0.095, \quad < tT >_{\rm cor} = 800. \end{aligned} \tag{10}$$

The results of the fits are presented in Tables **??** and 2. They are well inside reported error bars of the observed brightness temperatures at all frequencies and much better fit the observations than optical reference models (see Bastian et al. 1996 for a review).

Taking into account the parameters above we can simplify the Eq. (8). With $q << 1$ and $\tau_{\rm o} \equiv t_{\rm o}\lambda^2 << 1$ at $\lambda < t_{\rm o}^{-0.5} \simeq 10 - 18$ cm we can use the approximation $\Gamma(1-q,\tau_{\rm o}) \simeq 1$ and $\tau_{\rm o} << \tau_{\rm o}^q$ and obtain the total brightness spectrum

$$T_{\rm b,tot}(\lambda) = t_{\rm o}^q T_{\rm o}\lambda^{2q} + < tT_{\rm e} >_{\rm cor} \lambda^2. \tag{11}$$

The condition of $\tau_{\rm o} << 1$ is valid through the entire frequency range ($\nu > 10$ GHz) of chromosphere plage emission with dominating coronal contribution. At longer wavelengths one should use Eq. (8) with $T_{\rm b,chr} \simeq T_{\rm o}$. In Table 2 we give the observed and modelled brightness excess temperatures (ΔT) of a plage region relative to the quiet Sun

Table 2. Quiet Sun brightness T_b, observed and modelled

	Observed		Modelled	
ν (GHz)	T_{obs} (10^3 K)	σ_{obs} (10^3 K)	T_{mod} (10^3 K)	$T_{obs} - T_{mod}$ (10^3 K)
1.4	70.5	3.0	70.6	−0.1
1.6	63.8	2.8	58.6	5.2
1.8	52.2	2.5	50.0	2.2
2.0	42.9	1.9	43.5	−0.6
2.4	32.8	1.4	34.7	−1.9
2.8	27.1	1.1	29.1	−2.0
3.2	24.2	1.1	25.3	−0.9
3.6	21.7	1.1	22.5	−0.8
4.2	19.4	0.8	19.7	−0.3
5.0	17.6	0.8	17.2	0.4
5.8	15.9	0.7	15.6	0.3
7.0	14.1	0.6	14.0	0.1
8.2	12.9	0.6	13.0	−0.1
9.4	12.2	0.6	12.3	−0.1
10.6	11.3	0.5	11.7	−0.4
11.8	11.0	0.5	11.3	−0.3
13.2	10.8	0.5	10.9	−0.1
14.8	10.8	0.6	10.5	0.3
16.4	10.7	0.7	10.2	0.5
18.0	10.3	0.5	10.0	0.3
22.2	9.0	0.5	9.46	−0.5
36.8	7.8	0.5	8.40	−0.6
77.1	7.25	0.5	7.28	−0.03
87.0	7.2	0.5	7.11	0.09

brightness at different wavelengths, together with the observed and modelled quiet Sun brightness temperature (T_{QS}) and spectral index the $n(\lambda) = \mathrm{d}\log T_{b.pl}/\mathrm{d}\log\lambda$ for the modelled total brightness.

The polarized emission component $V(\lambda)$ can be now obtained from Eqs. (2) and (A12). For a simple model with constant magnetic field one can obtain for the chromosphere and corona:

$$V_{tot}(\lambda) = \beta_{chr} q t_o^q T_o \lambda^{2q} + \beta_{cor} < tT_e >_{cor} \lambda^2. \quad (12)$$

Here the magnetic fields are characterized by β_{cor} and β_{chr}.

4. Methods of magnetic field measurement

We now consider the problem of discrimination between the chromospheric and coronal contributions to the polarized emission at different wavelengths bands and discuss the appropriate methods for magnetic field estimates. We rewrite Eqs. (11)-(12) as

$$\begin{aligned} I_{obs} &= I_{chr} + I_{cor}, \\ V_{obs} &= V_{chr} + V_{cor} = \beta_{chr} q I_{chr} + \beta_{cor} I_{cor}, \end{aligned} \quad (13)$$

where

$$I_{chr} = \tau_o^q T_o, \quad \tau_o = t_o \lambda^2, \quad I_{cor} = < tT_e >_{cor} \lambda^2. \quad (14)$$

We note from Eqs. (13) that the contributions of the chromosphere and corona to intensity and polarization are different: if, for example, $\beta_{chr} = \beta_{cor}$, then the contribution of the chromosphere to V_{obs} is reduced by a factor q relative to contribution from corona. For $q \ll 1$, as found by our model, the reduction is significant. The chromospheric contribution both to intensity and polarization will always dominate the coronal contribution at shortest wavelengths, because the coronal brightness decreases faster (with λ^2) than that of the chromosphere (with λ^{2q}) - see Eq. (14). Thus, there are 3 typical frequency ranges (a, b and c): (a) the corona dominates both in intensity and polarization, (b) the chromosphere dominates both in intensity and polarization and (c) mixed regime with a dominating chromosphere in intensity and dominating corona in polarization.

Results of model calculations (Eqs. (13)-(14)) for a constant magnetic field (with $\beta_{chr} = \beta_{cor}$) are presented in Fig. 1 versus frequency for a plage region with parameters given in Eq. (10). As one can see from Fig. 1, clear dominance of either chromosphere or corona, both in intensity and polarization, exists only for high or low frequencies respectively. When one of these contributions becomes dominant, we can use Eqs. (13) and (14) (or Eq. 4) for magnetic field estimates in the corona and chromosphere:

$$[B_{cor}] = \frac{5350}{\lambda}\frac{V_{cor}}{I_{cor}}, \quad [B_{chr}] = \frac{5350}{\lambda}\frac{V_{chr}}{qI_{chr}}. \quad (15)$$

4.1. Coronal emission

At long cm-wavelengths the coronal contribution becomes significant (Fig. 1), so that we could use Eq. (15a) to estimate the coronal magnetic field. However, the magnetic field in the photosphere and the corona varies continuously. Therefore we establish, for a simplified model atmosphere, the relation between the value of an inhomogeneous field (or its parameter $\beta(h)$) at some height h and its estimated value $[\beta]$, as derived from Eq. (4). We show that for magnetic fields varying between the chromosphere and corona the estimate from Eq. (4) gives the value of the magnetic field at the height of the transition region (TR), i.e. near the base of the corona, independent from wavelength and the magnetic field profile.

We can approximate such an inhomogeneous atmosphere with a simplified model for $T_e(t)$ and $\beta(t)$ as

$$T_e(t) = T_{chr} + T_{cor} e^{-t/t_{cor}}, \quad \beta(t) = \beta_o(1 - e^{-t/t_\beta}). \quad (16)$$

This model may be treated as an atmosphere with an optically thick chromosphere ($T_{chr}(t) = \mathrm{const}$) and a hot corona ($T_{cor} >> T_{chr}$) with the optical depth $\tau_{cor} = \lambda^2 t_{cor}$ depending on the changing magnetic field. Its strength is constant ($\beta(t) = \beta_o$) in deep layers ($t > t_\beta$), with a rapid drop in the top layers ($t < t_\beta$), as it is expected for solar

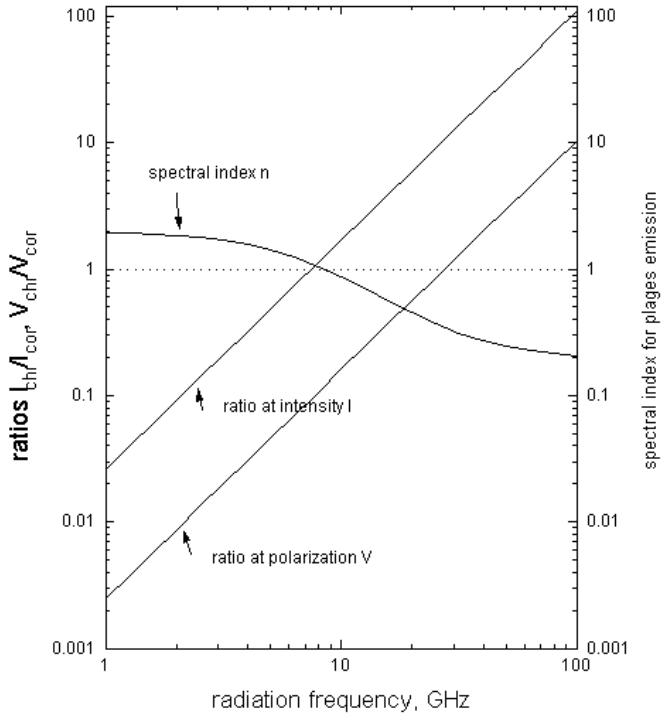

Fig. 1. The modelled relative contributions of chromospheric and coronae emission to intensity (Stokes parameter $I_{\rm chr}/I_{\rm cor}$) and polarization (Stokes parameter $V_{\rm chr}/V_{\rm cor}$) for the plage region atmosphere. The spectral index $n \equiv {\rm d}\log I_{\rm tot}/{\rm d}\log\lambda$ is calculated for the total intensity (Stokes parameter $I_{\rm tot} \equiv I_{\rm chr} + I_{\rm cor}$)

magnetic fields. The radiation transfer Eqs. (1)-(2) give then

$$I(\lambda) = T_{\rm chr} + \frac{\tau_{\rm cor}}{1+\tau_{\rm cor}} T_{\rm cor} \equiv I_{\rm chr} + I_{\rm cor}, \tag{17}$$

$$V(\lambda) = \beta_{\rm o} \frac{\tau_{\rm cor}}{(1+\tau_{\rm cor})^2} \frac{1}{1+(1+\tau_{\rm cor})t_\beta/t_{\rm cor}} T_{\rm cor}, \tag{18}$$

which leads to the estimate of the magnetic field through Eq. (4):

$$[\beta(\lambda)] \equiv \frac{V(\lambda)}{\lambda^2 {\rm d}I/{\rm d}(\lambda^2)} = \frac{1}{1+(1+\tau_{\rm cor})t_\beta/t_{\rm cor}} \beta_{\rm o}. \tag{19}$$

The following results (see also Grebinskij 1985) are typical for the polarization spectrum $V(\lambda)$ forming in an inhomogeneous medium:

(a) in any optically thick isothermal medium ($T_{\rm e} = T_{\rm chr}$), the radiation temperature ($T_{\rm rad}$) equals the kinetic temperature: $T_{\rm rad} = T_{\rm chr}$ (black body radiation), with the absence of polarization ($V_{\rm chr} = 0$);

(b) in the optically thin emission from the corona ($\tau_{\rm cor} << 1$) the polarization spectrum $V(\lambda)$ is proportional to the coronal brightness $I_{\rm cor} = \tau_{\rm cor} T_{\rm e,cor}$, and grows with λ^3, which is an observational signature of the coronal origin of polarization;

(c) in the optically thick regime ($\tau_{\rm cor} >> 1$) polarization quickly decreases, as for any black-body radiation;

(d) in the intermediate emission regime where $\tau \approx 1$ the polarization spectrum has a sharp maximum near wavelength $\lambda_{\rm cr}$ determined by $\tau_{\rm cor}(\lambda_{\rm cr}) \simeq 1$.

The bottom of the corona corresponds in our model to a normalised radiodepth of $t = t_{\rm cor}$ (Eq. 17), so that the model magnetic field strength $\beta(t_{\rm cor})$ at this level becomes:

$$\beta_{\rm TR} \equiv \beta_{\rm o}(1 - \exp(-t_{\rm cor}/t_\beta)), \tag{20}$$

so that the magnetic field (Eq. 16b) in the transition region is governed by $\gamma = t_{\rm cor}/t_\beta$:

$$\beta_{\rm TR} = \beta_{\rm o},\ \gamma >> 1; \quad \beta_{\rm TR} = \gamma\beta_{\rm o},\ \gamma << 1. \tag{21}$$

The estimated magnetic field (Eq. 19), as expected from the emission spectra (Eqs. 17, 18) through Eq. (4), corresponds to the model field at TR well. For an optically thin model corona (with $\tau_{\rm cor} << 1$), we find from Eq. (19):

$$[\beta(\lambda)] = \beta_{\rm o},\ \gamma >> 1; \quad [\beta(\lambda)] = \gamma\beta_{\rm o},\ \gamma << 1, \tag{22}$$

which are the same as for the simple model (Eqs. (16) and (21)). Thus, we conclude, that the method (Eq. 4) gives a field value corresponding to the coronal base near the transition region:

$$[\beta(\lambda)] \equiv \frac{V(\lambda)}{\lambda^2 {\rm d}I/{\rm d}(\lambda^2)} \simeq \beta_{\rm TR}. \tag{23}$$

4.2. Practical estimate methods

As was shown above, the main contribution to the polarized emission originates near the thin transition region. For this reason we can assume, that a magnetic field is uniform in the region of formation of polarized emission and use the equations above (Eq. (4) and Eqs. (13)) for the uniform case ($\beta_{\rm cor} = \beta_{\rm chr} = \beta_{\rm o}$), as a first approximation. Thus Eq. (4) can be used to estimate the magnetic field:

$$[B]_{\rm G} = 10700 \frac{\rho}{n\lambda_{\rm cm}}, \quad n \equiv \frac{{\rm d}\log I_{\rm obs}}{{\rm d}\log\lambda}, \quad \rho = \frac{V_{\rm obs}}{I_{\rm obs}}, \tag{24}$$

where n is the spectral index of the brightness temperature spectrum $I_{\rm obs}$, and $V_{\rm obs}$ is the observed radiative temperature of polarized emission. We present the typical values of the spectral index in Table **??** and Fig. 1.

From a single-frequency observation we have an another estimate for the magnetic field from Eqs. (13):

$$[B]_{\rm G} = 5350 \frac{1}{\lambda_{\rm cm}} Q(\lambda) \frac{V_{\rm obs}}{I_{\rm obs}}, \tag{25}$$

where we have introduced the scaling factor $Q(\lambda)$ as

$$Q = \frac{1+\frac{I_{\rm chr}}{I_{\rm cor}}}{1+q\frac{I_{\rm chr}}{I_{\rm cor}}}, 1 < Q < \frac{1}{q}. \tag{26}$$

Here $I_{\rm chr}$, $I_{\rm cor}$ are partial contributions to the total observed brightness $I_{\rm obs} = I_{\rm chr} + I_{\rm cor}$. For the case of a homogeneous magnetic field, the two estimates should give the same result, so that $n = 2/Q$.

From the single frequency observations of plage regions we are unable to determine either n or Q. They can be provided by our model simulation for observations (see Table **??** and Fig. 1). In addition, we can use simplified equations for the limiting cases at high and low emission frequencies:

(a) at long wavelengths with coronal domination in intensity $I_{\rm chr}/I_{\rm cor} << 1$ for $q << 1$, we have $Q \simeq 1$ and $n \simeq 2$ (optically thin coronal radiation), that Eq. (15) gives the magnetic field near the transition region:

$$[B]_{\rm G} = \frac{5350}{\lambda}\frac{V_{\rm obs}}{I_{\rm PL}},\ I_{\rm PL} \equiv \delta I_{\rm PL} + I_{\rm QS}, \qquad (27)$$

where $I_{\rm PL}$ is the observed total intensity of the plage region. The observed brightness excess $\delta I_{\rm PL}$ above the quiet Sun level $I_{\rm QS}$ is related to the coronal parameters by

$$< tT_{\rm e} >_{\rm PL} \simeq \lambda^{-2}\delta I_{\rm PL} + < tT_{\rm e} >_{\rm QS} . \qquad (28)$$

The value of $< tT_{\rm e} >_{\rm PL}$ is useful for checking if model and observations are consistent, because from a previous study (Bogod & Grebinskij 1997) we have a priori values for these parameters close to $< tT_{\rm e} >_{\rm PL} \simeq 900$ and $< tT_{\rm e} >_{\rm QS} \simeq 100$.

(b) chromospheric domination in intensity $I_{\rm chr}/I_{\rm cor} >> 1$ at short wavelengths. We have $Q >> 1$, because $q << 1$. In the limiting case $Q = 1/q$ and $n = 2q << 1$. This case may be important for measurements of umbral magnetic fields, where the observed polarization at the mm wave band may be extremely small for the relatively strong magnetic fields, due to the reduction of the coronal emission measure relative to plage areas as known from EUV observations.

In order to illustrate both limiting cases, we calculated typical values for the expected Q-factor for Westerbork ($\lambda = 6.0$ cm) and Nobeyama ($\lambda = 1.76$ cm) plage observations. We find for a typical plage area(s) $Q(\lambda = 6.0\ {\rm cm}) = 1.2$, and $Q(\lambda = 1.76\ {\rm cm}) = 3.9$. Therefore, with Nobeyama observations at 17 GHz the chromospheric contribution is important for more precise estimates.

5. Observational results

We review here several published and new observations, that are related to the problem of solar magnetic field measurements according the observations of microwave emission with high angular resolution.

5.1. RATAN and Westerbork observations between 1.5 and 11 GHz

(a) From RATAN observations of a bipolar spotless plage area (Bogod & Gelfreikh 1980) at $\lambda = 2.7$ and 3.2 cm (the most accurate measurements with RATAN on August 1, 1978) we obtained $\delta I = 5400$ and 7000 K, $V = 340$ and 380 K respectively. These values lead to estimates of $B = 57$ and 42 G through Eq. (27) and parameter check $< tT_{\rm e} >_{\rm PL} = 850$ and 790.

(b) From Westerbork observations (May 9-10, 1974) of isolated plages at $\lambda = 6$ cm, (see Fig. 10 of Kundu et al. 1977, the 3 plages labelled a, b and c), we have $\delta I = 30$, 40 and 30 (10^3 K) with $V = 8$, 12 and 12 (10^3 K). These values lead to estimates of $B = 60$, 100 and 80 G, and $< tT_{\rm e} >_{\rm PL} = 800$, 900 and 800.

(c) RATAN observations of the great prominence-coronal arcade structure above the W-limb on October 4, 1996 reveal the presence of a circularly polarized signal from the prominence location with $V/I = 0.03$ at $\lambda = 1.83$ cm (Bogod et al. 1998) which leads to a magnetic field strength of about $B = 50$ G.

(d) With RATAN multi-wavelength observations of a coronal hole area near the disc center (on October 12 and November 9, 1996) a weak polarization signal was registered with $V/\delta I = 0.015$ at $\lambda = 18.3$ cm (Borovik et al. 1999). At this wavelength the coronal hole was observed as a 30% brightness depression. This leads to a coronal parameter $< tT_{\rm e} >_{\rm CH} \approx 0.7 < tT_{\rm e} >_{\rm QS}$ and gives a magnetic field strength of about $B = 2.5$ G.

5.2. Nobeyama polarization observations at 17 GHz

Routine Nobeyama imaging techniques give polarization levels near the noise threshold for an active region with weak magnetic fields (see Shibasaki et al. 1991).

By averaging hundreds of separate images (Gelfreikh & Shibasaki 1998) a statistical polarization noise $V_{\rm rms}$ may be reduced to about 50 K with intensity signal up to 400 K for plage area(s) (at full brightness level $12000 - 14000$ K). Here we present results of such observations during June 1995 for the active region AR 7877 in intensity and polarization at 17 GHz (see Fig. 2).

AR 7877 (N09 E49) arose near the East limb on 5 June and it is developed to a bipolar sunspot group near central meridian time. From Kitt Peak photospheric magnetograms we saw a large scale background activity complex, with two adjacent bipolar regions, which we label as a, b, c, d from leading to trailing plage areas (see Fig. 2b). At the coronal heights, this complex of activity has an unusual magnetic structure, as delineated at soft X-rays with Yohkoh SXT observations (see Fig. 2a). From coaligning X-ray and magnetogram images we conclude, that X-rays "*butterfly*" originates from the region b, with two arcades (A, B) of magnetic flux lines, which emanate westword (labelled A) to region a and eastword (labelled B) to the region c. Nobeyama observations at polarization display four polarized regions labelled a–d (see Fig. 2e) which closely match photospheric magnetogram (see Fig. 2b), by position and signs (extraordinary emission mode) of polarization peaks. Peaks of polarized emission at locations a, b coincide with position of spots in the bipolar AR 7877, with strong magnetic fields up to 2500 G at photospheric level.

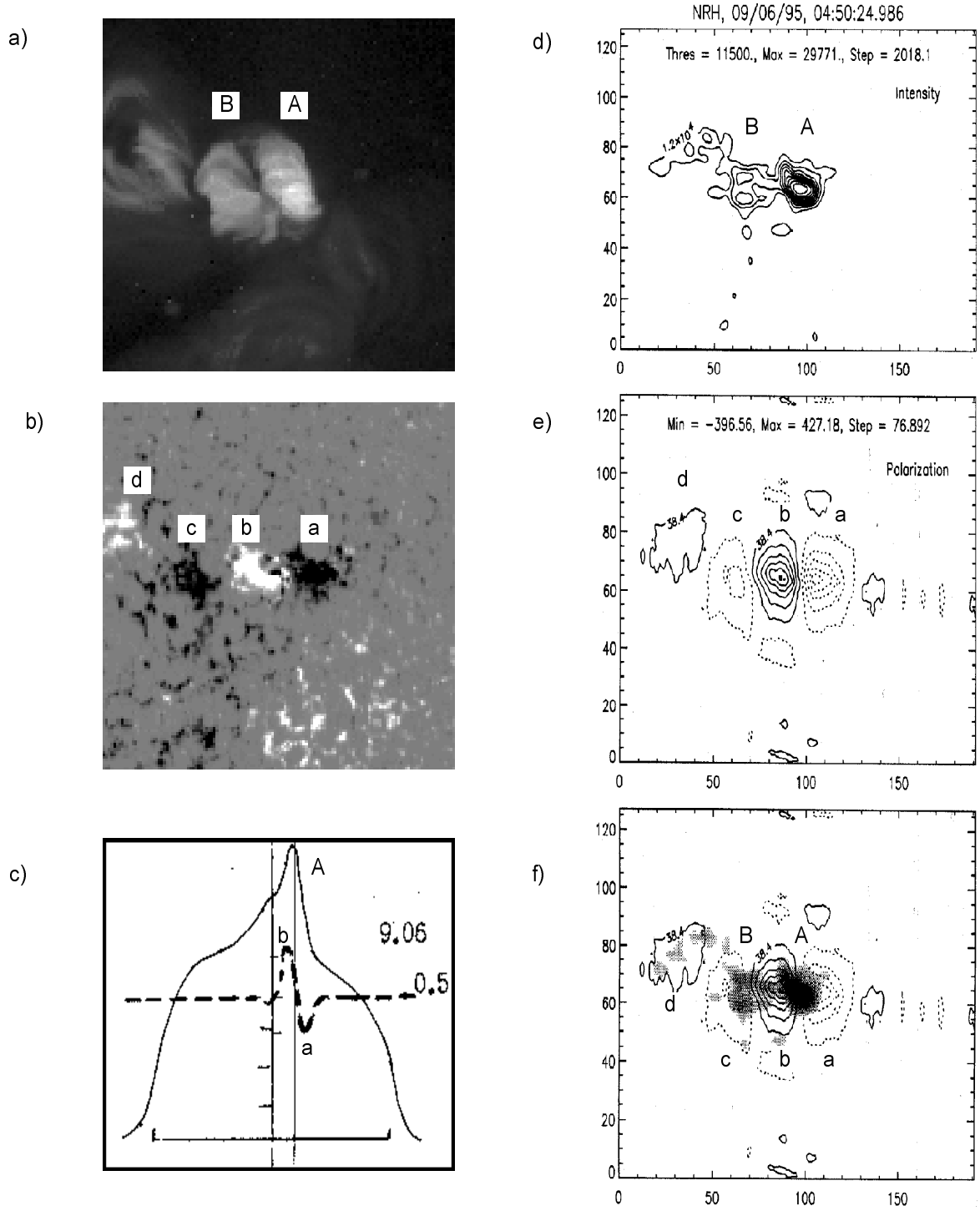

Fig. 2. Summary of the observations of AR 7877 on June 9, 1995. **a)** Yohkoh SXT image (600 × 600 arcsec), **b)** Kitt Peak magnetogram (fragment of 600 × 600 arcsec), **c)** microwave scan at $\lambda = 4.4$ cm with Great Pulkovo Radiotelescope of intensity (solid line) and circular polarization (dotted line) with HPBW = 60 arcsec, **d), e)** Nobeyama Radioheliograph images in intensity and circular polarization (50 images have been averaged), and **f)** its superposition. HPBW is about 15 arcsec, spatial scale unit for both axes is 4.9 arcsec per tickwork. For all images, solar north is on top and west is right. Nobeyama and Kitt Peak images are aligned to an accuracy about $10''$. The microwave peak brightness position coincides with the X-ray brightest loop top and is located on the neutral line both on the magnetogram and on microwave polarization

Nobeyma observations at intensity (see Fig. 2d) display, that the main brightness peaks do not overlay sunspot positions, but overlay the neutral line positions (see Fig. 2f for overlay of the I and V images). The same pattern is observed with Pulkovo 1D scan at longer wavelength $\lambda = 4.4$ cm (see Fig. 2c). We do not discuss here the nature of these weakly polarized emission peaks, which are possibly originate at the apex of X-ray arcades.

In context of microwave estimates of magnetic fields we conclude, taking into account the low brightness of plage areas observed at microwaves, that chromospheric magnetic fields at location of polarization peaks are below of cyclotron emission estimate for a third ($s = 3$) harmonic at $\lambda = 1.76$ cm (threshold of $B = 10700/s\lambda = 2000$ G).

Thus, we accept a thermal bremsstrahlung as emission mechanism at 17 GHz at the locations of all polarization peaks $a - d$, including sunspot plage areas. For two plage areas $a - b$ the measured values of intensity are $I = 16500$ K and 22000 K, with $I_{\rm QS} = 10^4$ K, and the polarization signals are $V = +430$ K and -400 K for, so that $\triangle I = 6500$ and 12000 K for areas a and b accordingly. For these plage areas we estimate a coronal parameter values $< tT_{\rm e} >_{\rm PL} = 1200$ and 1800. These values exceed the expected coronal values about $< tT_{\rm e} >_{\rm PL} = 800$, which suggest the hot X-ray loop contribution. If we adopt these values as coronal ones, then $< tT_{\rm e} >_{\rm PL} \lambda^2 = 3800$ K and 5600 K and the coronal contribution dominates the polarization. Thus, for a coronal magnetic field above these plage area(s) we would have $B = 93$ G and $B = 47$ G (Eq. 27). For plage c we obtain $\delta I = 4000$ K, $V = -145$ and an estimated field value $B = 51$ G.

For the same data, but by using the more strict estimate by Eq. (25), we would have a twofold increase of the magnetic fields at $a - c$ namely $B = 150$, 110 and 60 G respectively. These values are in good agreement with the photospheric values obtained from magnetograms made at Huiarou Station of BAO (courtesy of Prof. Hongqi Zhang), with peak values of approximately $B = 320$, 320 and 160 G for the same plage area(s).

6. Discussion and conclusions

In this paper we present for the first time a new approach to determine the solar magnetic fields of active regions based on measurements of the spectrum and polarization of the bremsstrahlung radio emission. In a number of previous studies this emission was analyzed either for the optically transparent coronal emission (spectral index $n = 2$) or for chromospheric structures. In the latter case the optical thickness is large and a weak polarization is due to the gradient of temperature, then the spectral index should be found from observations or taken a priori.

The new approach provides both chromospheric and coronal field values, if spectral intensity and polarization measurements are available. More than that the parameter $< tT >$, representing mostly the emission measure of the corona, can be found from the same observations. This was found to be in good agreement with our previous tomography study (Bogod & Grebinskij 1997).

As far as magnetic fields concerned the most important conclusion is the high value of the magnetic field in the corona above active regions. We found (in one example) the maximum values of $50 - 150$ G in plage areas (chromosphere-corona), while we derived $80 - 300$ G on optical magnetograms for the same active region. This implies a ratio of $0.6 - 0.7$ for radio to optical magnetic fields. It is of interest that similarly high ratios (up to 0.8) have been found for the magnetic fields above sunspots (see Shibasaki et al. 1994; Akhmedov et al. 1982), though the latter analysis was based on a different method, namely the usage of thermal cyclotron emission on the third harmonic of the electron gyrofrequency. This result is interpreted in terms of the very low height of the corona above sunspots.

From a methodical point of view, another important conclusion is the dominance of the coronal versus chromospheric contribution to the observed polarized component of solar emission below $\nu \approx 10$ GHz. The reason for the low contribution of the chromosphere to the polarized component is not model dependent and has a clear physical significance. The reason for the low degree of polarization of the chromospheric plasma is the low temperature gradients. So, both x-mode and o-mode are generated in layers with the same electronic kinetic temperature and produce the emission at brightness temperatures close to $< T_{\rm e} >$ with the result of $V \ll I$. The details of this effect certainly should be found from spectral-polarization observations with high spatial resolution. It is of practical interest that observations at $\lambda = 1.76$ cm made with V-maps Nobeyama radioheliograph include already significant parts of the chromospheric magnetic field. Additional information on the magnetic fields both in the corona and chromosphere can be gained from regular and high spatial resolution data, especially at 34 GHz with Nobeyama and 90 GHz with Metsähovi.

Our results show, that the measurements of brightness and circular polarization spectra of solar bremsstrahlung at microwaves give an efficient method to measure magnetic fields in the chromosphere and corona above active regions. However, to proceed significantly into this direction we still need large improvements both in imaging techniques (with high angular and spectral-polarization resolution) and interpretation (taking into account of spatial fine-structure effects).

Acknowledgements. This research has been partially supported by the Russian Foundation for Basic Research (RFBR) Projects 99-02-16403a and 99-02-16171a, INTAS - RFBR grants 95-316 and 97-1088.

Appendix A: Polarization transfer in inhomogeneous medium

The radiation transfer equations in the quasi-longitudinal approximation are decoupled for extraordinary-ordinary (+/−) circular modes with radiation temperature $T_{\rm b}^{\pm}$ (Zheleznyakov 1970).

$$\frac{{\rm d}T_{\rm b}^{\pm}}{{\rm d}\tau^{\pm}} = T_{\rm e} - T_{\rm b}^{\pm},$$
$$ {\rm d}\tau^{\pm} = {\rm d}\tau^{\rm o}\left(1 \pm \frac{2\nu_B\cos\alpha}{\nu}\right), \quad \frac{\nu_B}{\nu} \ll 1 \qquad \text{(A1)}$$

where ${\rm d}\tau^{\rm o} = \mu^{\rm o}{\rm d}l$, $\mu^{\rm o} \simeq 0.2\cdot\nu^{-2}N_{\rm e}^2T_{\rm e}^{-3/2}$ is the bremsstrahlung opacity in an isotropic plasma, $\nu_B = 2.8\ 10^6B$ the electron gyrofrequency, $\nu = c/\lambda$ and α the angle between the magnetic field $\boldsymbol{B}$ vector and the line of sight. For a plane-layer atmosphere $0 < l < L_{\rm o}$ Eq. (A1) can be integrated to obtain the observed brightness temperature

$$T_{\rm b}^{\pm} = \int_0^{\tau_{\rm o}^{\pm}} T_{\rm e}(\tau^{\pm}){\rm e}^{-\tau^{\pm}}{\rm d}\tau^{\pm} + {\rm e}^{-\tau_{\rm o}^{\pm}}T_{\rm ext}^{\pm}(\tau = \tau_{\rm o}^{\pm}). \qquad \text{(A2)}$$

where $T_{\rm ext}^{\pm}$ is an incident radiation temperature at the bottom $l = L_{\rm o}$ of the atmosphere.

For a single homogeneous layer $B(l) = B_{\rm o}$, $T_{\rm e}(l) = T_{\rm o}$, $N_{\rm e}(l) = N_{\rm o}$, $0 \le l \le L_{\rm o}$, with an optical depth $\tau_{\rm o}^{\pm}$ we obtain

$$T_{\rm b}^{\pm} = T_{\rm o} - (T_{\rm o} - T_{\rm ext}^{\pm}){\rm e}^{-\tau_{\rm o}^{\pm}}. \qquad \text{(A3)}$$

We consider the radiation transfer for the Stokes parameters $I = (T_{\rm b}^{+} + T_{\rm b}^{-})/2$ and circular polarization $V = (T_{\rm b}^{+} - T_{\rm b}^{-})/2$. After introducing definitions for $\beta = 2\nu_B\cos\alpha/\nu << 1$, $\tau_{\rm o} = (\tau_{\rm o}^{+} + \tau_{\rm o}^{-})/2$ and $T_{\rm ext}^{\pm} \equiv I_{\rm rad} \pm V_{\rm rad}$, we obtain in a linear approximation with respect to a small parameter $\beta_{\rm o}\tau_{\rm o}\exp(-\tau_{\rm o}) << 1$ the solutions for I and V as

$$I = T_{\rm o} - (T_{\rm o} - I_{\rm rad}){\rm e}^{-\tau_{\rm o}},$$
$$V = \beta_{\rm o}\tau_{\rm o}(T_{\rm o} - I_{\rm rad}){\rm e}^{-\tau_{\rm o}} + V_{\rm rad}{\rm e}^{-\tau_{\rm o}}. \qquad \text{(A4)}$$

We use this solution to construct a solution of the transfer equations in an inhomogeneous medium by summing up multi-layer solutions. For known spatial distributions of $T_{\rm e}(l)$, $N_{\rm e}(l)$, and $B(l)$ we introduce the frequency-independent radio depth $t(l)$ as a function of the current depth l, based on an isotropic optical depth $\tau(l)$

$$t(l) = \frac{1}{\lambda^2}\tau(l) = \frac{1}{\lambda^2}\int_0^l \mu^{\rm o}(l'){\rm d}l' \qquad \text{(A5)}$$

and express all spatial distributions as functions of the radio depth t. We decompose an atmosphere with a total radio depth $t_{\rm o} \equiv t(l = L_{\rm o})$ into a sum of n homogeneous layers with solutions given by (A4):

$$I_k = T_k - (T_k - I_{k+1}){\rm e}^{-\tau_k}, V_k = \beta_k\tau_k(T_k - I_{k+1}){\rm e}^{-\tau_k} \qquad \text{(A6)}$$

where $\tau_k = \lambda^2 t_k$ the radio depth, T_k the kinetic temperature for the k-th layer, and I_k, I_{k+1} the radiation temperature at the top and bottom of the k-th layer. For the total intensity at the top of the atmosphere we have to solve a pair of coupled equations for the Stokes parameters I and V

$$I = T_{\rm o} - \sum_{k=0}^{n}(T_k - T_{k+1})\exp\left(-\sum_{i=0}^{k}\tau_i\right),$$
$$V = \sum_{k=0}^{n}\beta_k\tau_k(T_k - I_{k+1})\exp\left(-\sum_{i=0}^{k}\tau_i\right). \qquad \text{(A7)}$$

To decouple the equations, we should express the $(T_k - I_{k+1})$ in terms of T_k by means of recurrent use of Eqs. (A6) as

$$(T_k - I_{k+1}) \equiv \triangle T_k + \sum_{i=1}^{\infty}\triangle T_{k+i}\exp(-\sum_{j=1}^{i}\tau_{k+j}), \qquad \text{(A8)}$$
$$\triangle T_k \equiv T_k - T_{k+1}.$$

After decoupling the Eqs. (A7) by means of substituting the term $(T_k - I_{k+1})$, in the limit of infinitesimal thin layers we can replace summation by integration, and in the limit of $t_{\rm tot} >> \lambda^{-2}$, find the solution of the radiation transfer equation:

$$I(\lambda) = \lambda^2\int_0^{\infty} T_{\rm e}(t){\rm e}^{-\lambda^2 t}{\rm d}t \qquad \text{(A9)}$$

$$V(\lambda) = \lambda^2\int_0^{\infty}\beta(t)\triangle T(t){\rm e}^{-\lambda^2 t}{\rm d}t,$$
$$\triangle T(t) = \int_0^{\infty}\frac{{\rm d}T_{\rm e}(t+t')}{{\rm d}t}{\rm e}^{-\lambda^2 t'}{\rm d}t'. \qquad \text{(A10)}$$

In the case of a homogeneous magnetic field distribution $B(l) = B_{\rm o}$ the radiation transfer Eq. (A1) depends on frequency and magnetic field only through the combination $\lambda^2(1 \pm \frac{1}{2}\beta_{\rm o})$. Therefore, its solution is ruled by a scaling law

$$T_{\rm b}^{\pm}(\lambda^2) = I(\lambda^2(1 \pm \frac{1}{2}\beta_{\rm o})) \simeq I(\lambda^2) \pm \frac{1}{2}\beta_{\rm o}\lambda^2\frac{{\rm d}I}{{\rm d}\lambda^2}, \qquad \text{(A11)}$$

and the polarization spectrum is determined by the differential equation

$$V(\lambda) = \beta_{\rm o}\lambda^2\frac{{\rm d}I}{{\rm d}\lambda^2}, \quad V(\lambda) = -\int_0^{\infty}\frac{t{\rm d}T_{\rm e}(t)}{{\rm d}t}{\rm e}^{-\lambda^2 t}\lambda^2{\rm d}t. \qquad \text{(A12)}$$

These equations have been derived before in a similar form (Bogod & Gelfreikh 1980; Grebinskij 1985) without discussions of its applicability.

Appendix B: Scaling law for free-free brightness depression

From the EUV observations is well known, that solar atmosphere has significant emission measure in the temperature range, intermediate between coronal-chromospheric values. It should lead to significant contribution to microwave emission, contrary to observations (see Zirin et al. 1991 for review).

As was proposed by Grebinskij (1987), this dilemma may be solved, if one takes into account the spatial inhomogeneity of atmosphere. Following that paper, we clarify this conclusion with simple scaling laws for model example of isothermal plasma volume with some electron temperature $T_\mathrm{o} = \mathrm{const}$, and some fixed value of emission measure $EM_\mathrm{o} = \mathrm{const}$. We show, that observed microwave $f - f$ emission brightness T_eff of such plasma is strongly dependent on spatial inhomogeneity and becomes negligible for strong inhomogeneity.

We compare two spatial configurations, in the same projected area, say $S_\mathrm{o} = L_\mathrm{o} \times L_\mathrm{o}$, with depth h_o. At homogeneous case, with $N_\mathrm{e}(\boldsymbol{r}) = \mathrm{const} = N_\mathrm{o}$, we have for total emission measure $EM_\mathrm{tot} = N_\mathrm{o}^2 L_\mathrm{o}^2 h_\mathrm{o}$. As the model inhomogeneity, we assume *en ensemble* of some number K of horizontal slabs with dimensions $L_\mathrm{o} \times d \times d$ and constant number density $N_\mathrm{e}(\boldsymbol{r}) = \mathrm{const} = N_*$ inside and zero outside each slab, with the same $EM^*_\mathrm{tot} = K N_*^2 L_\mathrm{o} d^2 = EM_\mathrm{tot}$, and total projected area $S_* = K L_\mathrm{o} \times d$. From the EM balance, one would have

$$N_*^2 d = \frac{L_\mathrm{o}^2}{K L_\mathrm{o} d} \equiv \frac{1}{\varepsilon} N_\mathrm{o}^2 h_\mathrm{o} \tag{B1}$$

where $\varepsilon \equiv S_*/S_\mathrm{o}$ is a surface filling factor. Now, we consider the normalized optical depth $t \equiv \tau(\lambda = 1\ \mathrm{cm})$ along the line of sight for both configurations, as

$$t_\mathrm{o} \equiv k' N_\mathrm{o}^2 h_\mathrm{o},\ t_* \equiv k' N_*^2 d,\ k' = \mathrm{const} \tag{B2}$$

and, taking into account Eq. (B1), we find a scaling law for optical depth

$$t_* = \frac{1}{\varepsilon} t_\mathrm{o},\ \varepsilon \leq 1. \tag{B3}$$

Here it is crucial, that we have only one slab at the line of sight, if condition $\varepsilon \leq 1$ fulfilled (from contrary: if total surface $S_* > S_\mathrm{o}$, then slabs *should overlap,* because they do not match projected area). Now, we find a scaling law for the horizontally smoothed observed microwave brightness $< T_\mathrm{b} >$ as:

$$< T_\mathrm{b} >_\mathrm{o} \equiv T_{\mathrm{b,o}} = T_\mathrm{o}(1 - \mathrm{e}^{-t_\mathrm{o}\lambda^2}), \tag{B4}$$

$$< T_\mathrm{b} >_* \equiv \varepsilon T_{b,\varepsilon} = \varepsilon T_\mathrm{o}(1 - \mathrm{e}^{-t_\mathrm{o}\lambda^2/\epsilon}) \tag{B5}$$

which are correct for $\varepsilon \leq 1$ condition and becomes same at $\varepsilon = 1$.

Equations (B1)-(B5) reveal a scaling nature of brightness depression, irrespective of detailed spacing of microscale structures: if the filling factor is sufficiently small (i.e. $\varepsilon << 1$, and $t_\mathrm{o}\lambda_*^2/\epsilon > 1$), then at some wave band $\lambda \geq \lambda_*$ we have: $< T_\mathrm{b} >_* = \varepsilon T_\mathrm{o} << T_\mathrm{o}$. At the shorter wave band $\lambda \leq \lambda_*$ with $t_\mathrm{o}\lambda^2/\epsilon < 1$, the emission is optically thin and does not depend on inhomogeneity, but remains reduced as $< T_\mathrm{b} >_* = < T_\mathrm{b} >_\mathrm{o} = t_\mathrm{o}\lambda^2 T_\mathrm{o} << T_\mathrm{o}$.

These scalings, together with the observed small EUV-filling factors $\varepsilon << 1$, solves the problem of consistency results of optical and microwave observations: at EUV band we have optically thin emission, proportional to emission measure, but we never detect it at microwaves, with depressed brightness at the optically-thick regime (with $t_\mathrm{o}\lambda^2 << 1$, but $t_\mathrm{o}\lambda^2/\epsilon >> 1$ at the cm waveband).

References

Abramov-Maksimov V.E., Vyalshin G.F., Gelfreikh G.B., Shatilov V.I., 1996, Solar Phys. 164, 333

Akhmedov Sh.B., Gelfreikh G.B., Bogod V.M., Korzhavin A.N., 1982, Solar Phys. 79, 41

Alissandrakis C.E., Kundu M.R., Lantos P., 1980, A&A 82, 30

Apushkinskiy G.P., Topchilo N.A., 1976, AZh 20, 393

Avrett E.H., 1997, in Solar Electromagnetic Radiation Study for Solar Cycle 22, Pap J.M., Frohlich C. and Ulrich R.K. (eds.). Kluwer Academic Publishers

Bastian T.S., Dulk G.A., Leblanc Y., 1996, ApJ 473, 539

Benz A.O., Krucker S., Acton W., Bastian T.S., 1997, A&A 320, 993

Bogod V.M., Gelfreikh G.B., 1980, Solar Phys. 67, 29

Bogod V.M., Grebinskij A.S., 1997, Solar Phys. 176, 67

Bogod V.M., Grebinskij A.S., Garaimov V.I., 1998, Solar Phys. 182, 139-143

Borovik V.N., Medar V.G., Korzhavin A.N., 1998, AZh 25, 299-307

Fontenla J.M., Avrett E.H., Loeser R., 1993, ApJ 406, 319

Gary D.E., Hurford G.J., 1994, ApJ 420, 903

Gelfreikh G.B., 1972, Astronomichskij Cirkular, No. 699, 3

Gelfreikh G.B., Shibasaki K., 1998, CESRA Meeting Abstracts, Espoo, HUT-MET-27, 39

Grebinskij A.S., 1985, Astron. Zh. 62, 768

Grebinskij A.S., 1987, Sov. Astr. Lett. 13, 4

Grebinskij A., Shibasaki K., Zhang H., 1999, Solar Physics with Radio Observations, Proc. of Nobeyama Symp. 1998, NRO Report

Kundu M.R., Alissandrakis C.E., Bregman J.D., Hin A.C., 1977, ApJ 213, 278

Lang K.R., Willson R.F., Kile J.N., et al., 1993, ApJ 419, 398

Lee J., White S.M., Kundu M.R., Mikic Z., 1999, Solar Physics with Radio Observations, Proc. of Nobeyama Symp. 1998, NRO Report

McClymont A.N., Jiao L., Mikic Z., 1997, Solar Phys. 174, 191

Hanaoka Y., Shibasaki K., Nishio M., et al. (17 total), 1994, NRO Report, No. 357, 35

Ratcliffe J.A., 1959, Magneto-Ionic Theory and Its Applications to the Ionosphere. University Press, Cambridge

Shibasaki K., Kai K., Enome S., et al., 1991, in Environmental and Space Electromagnetics, Kikuchi H. (ed.). Springer-Verlag, Berlin, p. 345
Shibasaki K., Enome S., Nakajima H., et al., 1994, PASJ 46, L17
Urpo S., Hildebrandt J., Kruger A., 1987, Solar Phys. 112, 119
Yan Y., Sakurai T., 1997, Solar Phys. 174, 65
Vourlidas, Bastian, Ashwanden, 1997, ApJ 489, 403
White S.M., Kundu M.R., 1997, Solar Phys. 174, 31
Zheleznyakov V.V., 1970, Radio Emission of the Sun and Planets. Pergamon Press, New York
Zirin H., Baumert B.M., Hurford G.J., 1991, ApJ 370, 779